JOC The Journal of Organic Chemistry

Article

pubs.acs.org/joc

Near-Silence of Isothiocyanate Carbon in ^{13}C NMR Spectra: A Case Study of Allyl Isothiocyanate

Rainer Glaser,* Roman Hillebrand, Wei Wycoff, Cory Camasta, and Kent S. Gates

Department of Chemistry, University of Missouri, Columbia, Missouri 65211, United States

Supporting Information

ABSTRACT: ^{1}H and ^{13}C NMR spectra of allyl isothiocyanate (AITC) were measured, and the exchange dynamics were studied to explain the near-silence of the ITC carbon in ^{13}C NMR spectra. The dihedral angles $\alpha = \angle$(C1−C2−C3−N4) and $\beta = \angle$(C2−C3−N4−C5) describe the *conformational dynamics* (conformation change), and the bond angles $\gamma = \angle$(C3−N4−C5) and $\varepsilon = \angle$(N4−C5−S6) dominate the *molecular dynamics* (conformer flexibility). The conformation space of AITC contains three minima, C_s-M1 and enantiomers M2 and M2′; the exchange between conformers is very fast, and conformational effects on ^{13}C chemical shifts are small ($\nu_{M1} - \nu_{M2} < 3$ ppm). Isotropic chemical shifts, ICS(γ), were determined for sp, sp^x, and sp^2 N-hybridization, and the γ dependencies of δ(N4) and δ(C5) are very large (10−33 ppm). Atom-centered density matrix propagation trajectories show that every conformer can access a large region of the potential energy surface AITC(γ,ε,...) with 120° < γ < 180° and 155° < ε < 180°. Because the extreme broadening of the ^{13}C NMR signal of the ITC carbon is caused by the structural flexibility of every conformer of AITC, the analysis provides a general explanation for the near-silence of the ITC carbon in ^{13}C NMR spectra of organic isothiocyanates.

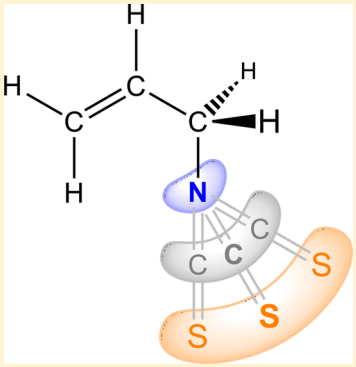

1. INTRODUCTION

Isothiocyanates (ITCs) are phytochemicals released from cruciferous vegetables, and they have been receiving considerable interest due to their health benefits.[1−6] For instance, isothiocyanates have been shown to reduce hyperglycemia in mice[7] and lower the risk of chemical carcinogenesis in various animal models.[8] ITCs react readily with thiols, and many of the biological effects of these agents arise via covalent modification of key cysteine residues on cellular proteins.[9] In the course of our investigations of the reaction of allyl isothiocyanate (allyl-ITC, AITC, also known as 3-isothiocyanatopropene) with protein thiols, we noticed the surprising absence of the isothiocyanate carbon C5 in the ^{13}C NMR spectrum of AITC (Figure 1 and Scheme 1).

The ^{13}C NMR spectrum of allyl isothiocyanate shows the expected peaks for C1−C3, and the dynamic nature of the molecule causes modest line broadening, reflecting the variable environment of these C centers. In contrast, however, the isothiocyanate C (C5) is not just broadened; it is nearly silent (i.e., almost flattened) in the ^{13}C NMR of AITC. A review of spectra of organic isothiocyanates in the Sigma-Aldrich catalog[10] (SAC) and in the Spectral Database for Organic Compounds[11] (SDBS) showed this phenomenon to be quite general. Indeed, the carbon resonance for the isothiocyanate group is nearly silent in the spectra of organic isothiocyanates R−N═C═S (i.e., R = phenyl,[12] benzyl,[13] butyl,[14] and many others) or not observed at all (i.e., R = propyl[15]). The low intensity of the ITC carbon signal was noticed by Jones and Allen in their ^{13}C NMR study of para-substituted phenyl isothiocyanates[16] and by Giffard et al. in NMR studies (^{1}H, ^{13}C, ^{15}N) of organic isothiocyanates R−NCS (R = methyl, butyl, phenyl, vinyl).[17] Both groups attributed the low intensity of the ITC carbon signal to quadrupolar broadening by ^{14}N. We note that no unusual broadening occurs for the α-C in these compounds and offer an alternative explanation for the low intensity of the ITC carbon signal in organic isothiocyanates.

Here, we report the results of a theoretical study of the conformational and molecular dynamics of AITC to explain the observed NMR spectra. The *conformational dynamics* (i.e., the fast exchange *between* conformations) are due to changes of the dihedral angles $\alpha = \angle$(C1−C2−C3−N4) and $\beta = \angle$(C2−C3−N4−C5), whereas the *molecular dynamics* (i.e., the structural flexibility *within* each conformer) are due to facile changes of the bond angles at N4, $\gamma = \angle$(C3−N4−C5), and at C5, $\varepsilon = \angle$(N4−C5−S6). Potential energy surface analysis and molecular dynamics studies show that the near-silence of C5 in the ^{13}C NMR spectrum is caused by the facile change of the N-hybridization in the wide range of 120° < γ < 180° in every conformation of AITC. Because the extreme broadening of the ^{13}C NMR signal of the ITC carbon is caused by the structural flexibility of the minimum structures, the analysis of AITC provides a general explanation for the (near-)silence of the ITC carbon in ^{13}C NMR spectra of unaggregated and sterically unencumbered organic isothiocyanates.

Received: January 12, 2015
Published: April 17, 2015

DOI: 10.1021/acs.joc.5b00080
J. Org. Chem. 2015, 80, 4360−4369

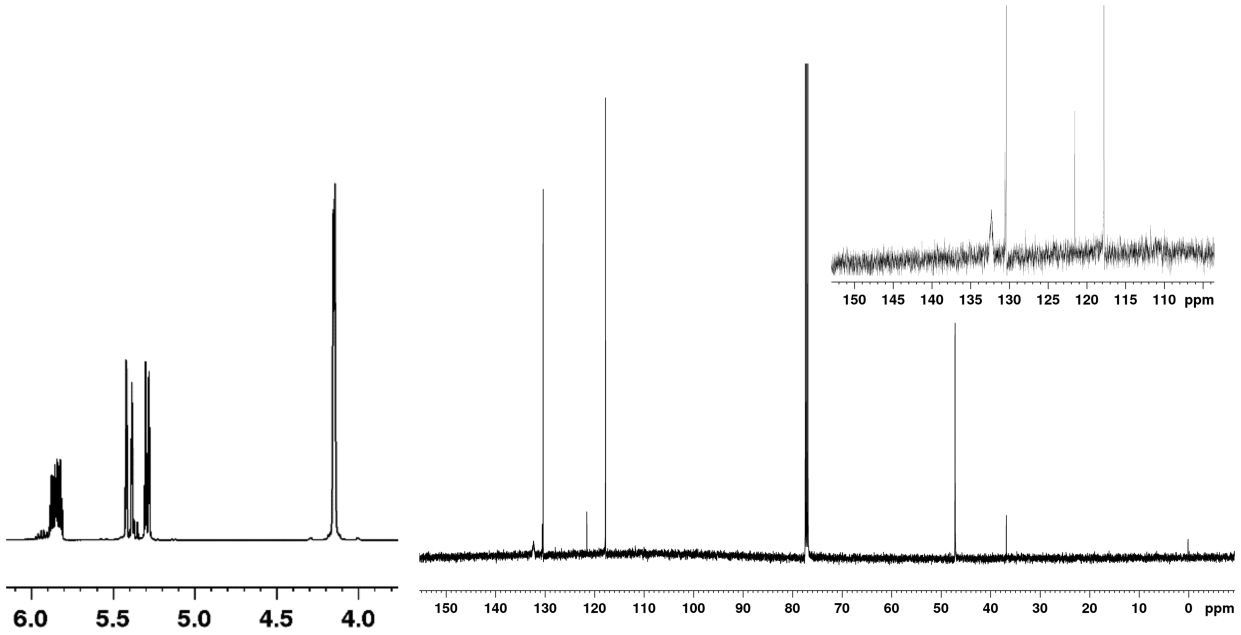

Figure 1. ^{1}H and ^{13}C NMR spectra of allyl isothiocyanate in $CDCl_3$. The ^{1}H NMR spectrum (left) shows the expected vinylic and allylic peaks at chemical shifts δ of 5.85 (H_a), 5.40 (H_b), 5.29 (H_c), and 4.14 ($H_{d,e}$) ppm. The ^{13}C NMR spectrum shows three well-defined peaks at chemical shifts δ of 130.26 (C2), 117.65 (C1), and 47.04 (C3) ppm but no clear peak for the ITC carbon C5. The inset in the top right shows an expanded view of the ^{13}C NMR spectrum in the region of 130 ± 40 ppm.

Scheme 1. Atom Numbering of Allyl Isothiocyanate

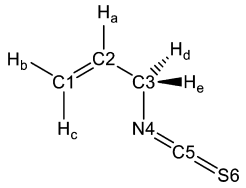

2. RESULTS AND DISCUSSION

2.1. Solvent Effects on NMR Spectra and Correlation Spectroscopy. Chemical shifts of AITC were measured in the solvents $CDCl_3$, CD_3OD, and DMSO-d_6 (Table 1). The ITC carbon gives a very broad signal in ^{13}C NMR spectra. We measured the HMBC spectrum[18b,19b] in $CDCl_3$ (Figure 2) to establish that the very broad peak at δ 133.3 ppm is in fact due to C5(AITC).

Table 1. ^{1}H and ^{13}C NMR Measurements of AITC

parameter	$CDCl_3$[a]	CD_3OD	DMSO
ε[b]	4.7133	32.613	46.826
$\delta(H_a)$[c]	5.85	5.94	5.94
$\delta(H_b)$	5.40	5.39	5.36
$\delta(H_c)$	5.29	5.28	5.27
$\delta(H_{d,e})$	4.15	4.36	4.36
δ(C1)	117.65	115.87	117.18
δ(C2)	130.26	131.02	131.87
δ(C3)	47.04	46.45	47.18
δ(C5)	132.30	129.90	129.84

[a]Coupling constants (Hz) in $CDCl_3$: J_{ab} = 10.0, J_{ac} = 16.8, and J_{bc} = 5. [b]Dielectric constant ε of the solvent. [c]Chemical shifts (ppm) relative to TMS.

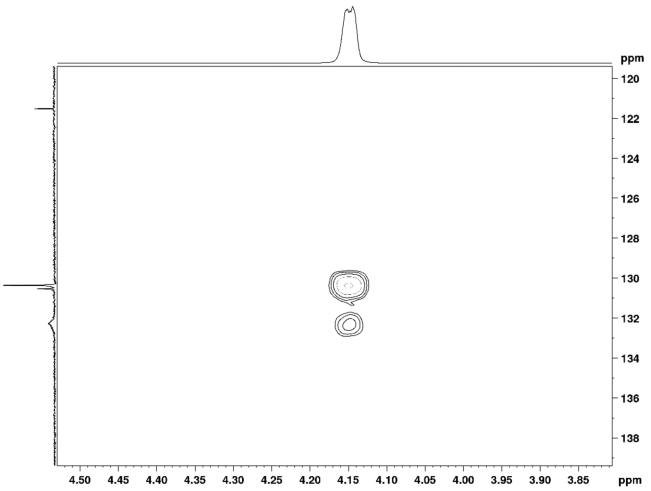

Figure 2. Heteronuclear multiple-bond correlation (HMBC) spectroscopy of AITC in $CDCl_3$ shows long-range coupling between the methylene hydrogen atoms $H_{d,e}$ at δ = 4.15 ppm and C5 at δ = 133.3 ppm.

Solvent effects on chemical shifts are generally small (^{1}H NMR, $\Delta\delta_{solv}$ < 0.22 ppm; ^{13}C NMR, $\Delta\delta_{solv}$ < 1.80 ppm). The weak C5 peak appears close to the C1 peak, and their sequence is solvent-dependent; C5 occurs at a slightly higher chemical shift in $CDCl_3$ (δ(C5) > δ(C1)), while it appears at a slightly lower chemical shift in donor solvents.

2.2. Potential Energy Surface Analysis of AITC. The potential energy surface (PES) of AITC was explored at the B3LYP/6-311G(d,p) level, and eight stationary structures were determined (Scheme 2 and Figure 3). Results of the PES analysis are listed in Table 2, and these include the frequencies of the three lowest vibrational modes, the total energy, and the molecular thermal energy and entropy. Important structural data of the stationary structures are listed in Table 3, and

DOI: 10.1021/acs.joc.5b00080
J. Org. Chem. 2015, 80, 4360−4369

Scheme 2. Schematic Drawings of Stationary Structures Studied

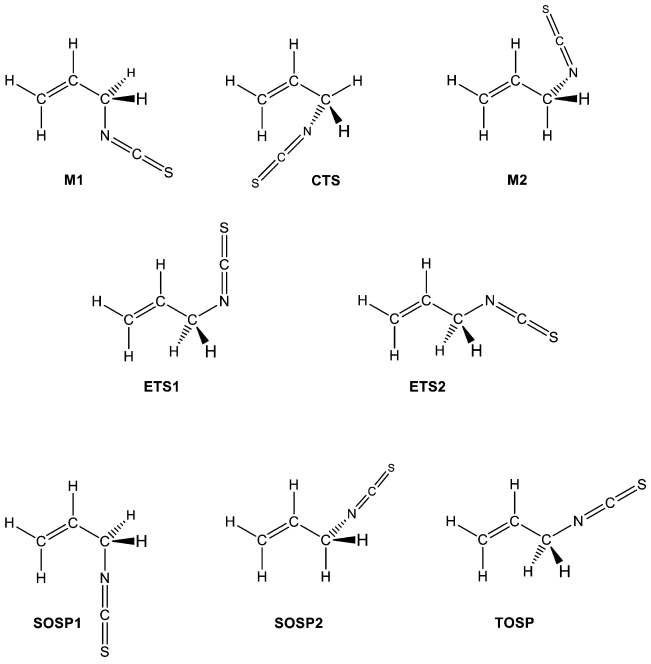

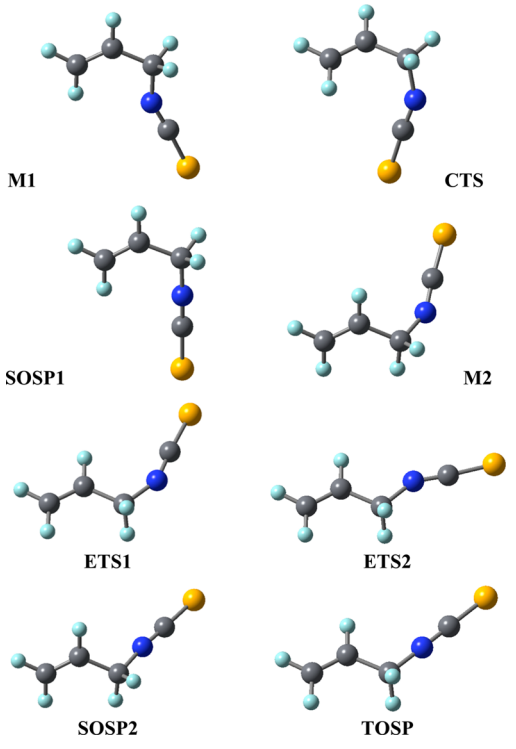

Figure 3. Molecular models of the B3LYP/6-311G(d,p) optimized stationary structures of AITC. The best plane of the C_3 moiety is rotated in or out of the paper plane.

Cartesian coordinates of the structures are provided as Supporting Information. Relative energies and relative free enthalpies are collected in Table 4 (vide infra).

The conformations about the C2−C3 and C3−N4 bonds are described by the dihedral angles $\alpha = \angle(C1{-}C2{-}C3{-}N4)$ and $\beta = \angle(C2{-}C3{-}N4{-}C5)$, respectively, and their values are listed in Table 3. We are particularly interested in the structural dynamics due to the variable N-hybridization and NCS bending, and hence, Table 3 also contains the bond angles at N ($\gamma = \angle(C3{-}N4{-}C5)$) and at C5 ($\varepsilon = \angle(N4{-}C5{-}S6)$), the two bond lengths involving N, d(C3−N4) and d(N4═C5), as well as the bond length d(C5═S6).

The potential energy surface of AITC contains three minima: C_s-symmetric M1 and a pair of enantiomers M2 and M2′ (Figure 3). The vinyl group eclipses the C3−N4 bond in M1 and one of the C3−H bonds in M2 and M2′. M1 is cis about the C2−C3 bond with $\alpha = 0.0°$, and M2 is gauche with $\alpha = 123.2°$. M1 adopts a trans conformation about the C3−N4 bond ($\beta = 180.0°$), and one wonders whether a structure M3 might exist with $\alpha \approx 0°$ and $|\beta| \approx 60°$. Careful searches for such a minimum all led directly to M2 with $\alpha = 123.2°$ and $\beta = 17.1°$.

A scan of the potential energy surface starting at M1 and incrementing the dihedral angle β stepwise by 5° shows that the rotation about the C3−N4 bond is coupled to the simultaneous rotation of the vinyl group around the C2−C3 bond. This PES scan traces the isomerization path from M1 to M2 (or M2′) via the transition state structure CTS. This isomerization involves changes of the conformations about both the C2−C3 and C3−N4 bonds, but none of the structures along the rotational path showed drastic changes of the N-hybridization with $\gamma \approx 150 \pm 3°$.

Vibrational analysis shows the C_s-symmetric structures ETS1 ($\alpha = 180°$, $\beta = 0°$) and ETS2 ($\alpha = 180°$, $\beta = 180°$) to be transition state structures for enantiomerization between M2 and M2′. The structures ETS1 and ETS2 again feature angles at N ($\gamma \approx 150°$) that are indicative of sp^x-hybridization with $1 < x < 2$. The higher-order saddle point structures SOSP1, SOSP2, and TOSP were located to explore the consequences of linearization and sp-hybridization at N. It is of interest to compare the properties of these stationary structures to structures with $\gamma \approx 120°$. Because there are no stationary structures with $\gamma \approx 120°$, we optimized structures of the types M1, M2, CTS, ETS1, and ETS2 with the imposed constraint of $\gamma = 120°$. The resulting structures are identified by the appended subscript "120", and their data are included in Tables 2−4.

All of the stationary structures are very close in energy (Table 4)—within 3 kcal/mol—and this is also true for all of the structures along the scans of the rotational profiles. Hence, AITC is conformationally flexible, and conformational isomerization involves rotations about both the C2−C3 and C3−N4 bonds. Moreover, we also know that the minima, the transition state structures, and the higher-order saddle points all are close in energy, and thus, the *accessible conformational space involves a much larger region of the potential energy surface* than merely the immediate vicinity of the minima and narrow corridors along the intrinsic reaction paths connecting minima and transition states. For example, the second-order saddle point structures SOSP1 and SOSP2 are just slighly less stable than M1 or M2 (Table 4), respectively. Similarly, enantiomerization between M2 and M2′ does not have to pass through ETS1 or ETS2 and may proceed instead along any number of paths, including paths traversing the TOSP region ($\gamma \approx 180°$). The PES analysis shows that "the conformations of AITC" are not well-represented by the stationary structures of M1 and M2 alone. Because of the molecular flexibility of the conformers, it is more appropriate and necessary to represent their structures by the regions around the stationary structures M1 and M2 and to

DOI: 10.1021/acs.joc.5b00080
J. Org. Chem. 2015, 80, 4360−4369

Table 2. Total Energies, Thermochemistry, and Character of Stationary Structures of AITC

type	f_1[a,b]	f_2	f_3	energy[c]	TE[d]	S[e]	E_{120}[c]
M1	27	60	180	−608.423444	55.32	85.34	−608.417885
M2	18	69	118	−608.422968	55.46	86.57	−608.417077
CTS	−151	31	57	−608.419110	54.85	82.80	−608.417388
ETS1	−135	30	55	−608.419829	54.70	83.00	−608.411660
ETS2	−120	30	63	−608.419943	54.62	82.09	−608.414322
SOSP1	−67	−43	168	−608.422795	54.20	75.21	
SOSP2	−72	−45	108	−608.422032	54.25	75.84	
TOSP	−140	−53	−47	−608.419265	53.52	72.54	

[a]Character of stationary structure and number of imaginary vibrational frequencies: minimum, 0; transition state, 1; second-order saddle point, 2; third-order saddle point, 3. [b]Wavenumbers f_i (in cm^{-1}) of the three lowest vibrational modes. [c]Energy in atomic units. Energy E_{120} refers to the structure of the same type but optimized with $\gamma = 120°$. See text for details. [d]Thermal energy (TE) in kcal/mol. [e]Molecular entropy S in cal/(K mol)$^{-1}$.

Table 3. Pertinent Structural Parameters of Stationary Structures of AITC[a−c]

Type	α	β	γ	ε	d(C−N)	d(N═C)	d(C═S)
M1	0.0	180.0	149.7	176.3	1.4328	1.1872	1.5897
M2	−123.2	−17.0	150.1	176.1	1.4402	1.1873	1.5912
CTS	59.7	−11.7	150.5	176.4	1.4387	1.1866	1.5912
ETS1	180.0	0.0	151.0	176.3	1.4324	1.1864	1.5916
ETS2	180.0	180.0	149.3	176.2	1.4362	1.1875	1.5900
SOSP1	0.0	0.0	178.3	179.8	1.4162	1.1768	1.5975
SOSP2	−125.5	176.9	174.6	179.3	1.4240	1.1771	1.5979
TOSP	180.0	0.0	179.5	179.9	1.4188	1.1766	1.5980
$M1_{120}$	0.0	180.0	120.0	176.5	1.4818	1.2097	1.5770
$M2_{120}$	121.1	79.5	120.0	176.4	1.4944	1.2101	1.5785
CTS_{120}	124.0	−93.7	120.0	176.5	1.4938	1.2100	1.5775
$ETS1_{120}$	180.0	0.0	120.0	174.6	1.4880	1.2118	1.5791
$ETS2_{120}$	180.0	180.0	120.0	176.5	1.4852	1.2101	1.5769
CSD, min[d]			141.5	172.6	1.360	1.046	1.473
CSD, max[d]			176.2	179.2	1.466	1.183	1.598
CSD, av[d]			159.3	176.2	1.441	1.152	1.572
CSD, std dev[d]			10.6	1.9	0.024	0.027	0.024

[a]Dihedral angles $\alpha = \angle$(C1−C2−C3−N4) and $\beta = \angle$(C2−C3−N4−C5) in degrees. [b]Bond angles $\gamma = \angle$(C3−N4−C5) and $\varepsilon = \angle$(N4−C5−S6) in degrees. [c]Bond lengths in angstroms. [d]Summary of alkyl isothiocyanate crystal structures in the Cambridge Structural Database (CSD).

Table 4. Relative and Activation Energies[a,b]

parameter	ΔE	ΔG_{298}	parameter	ΔE
E_{rel}, M2 vs M1	0.30	0.06	E_{rel}, $M1_{120}$ vs M1	3.49
E_{act}, ETS1 vs M2	1.97	2.28	E_{rel}, $M2_{120}$ vs M2	3.70
E_{act}, ETS2 vs M2	1.90	2.40	E_{rel}, CTS_{120} vs CTS	1.08
E_{act}, CTS(M2,M1)	2.42	2.94	E_{rel}, $ETS1_{120}$ vs ETS1	5.13
E_{act}, CTS(M1,M2)	2.72	3.00	E_{rel}, $ETS2_{120}$ vs ETS2	5.43
E_{rel}, SOSP1 vs M1	0.41	2.30		
E_{rel}, SOSP2 vs M2	0.59	2.59		
E_{rel}, TOSP vs ETS1	0.35	2.29		

[a]$\Delta H_{298} = \Delta E + \Delta TE$. $\Delta G_{298} = \Delta H_{298} - T\Delta S_{298}$. [b]All values in kcal/mol.

realize that *these regions contain all kinds of structures with 120° < γ < 180°*.

We searched the Cambridge Structural Database[20] (CSD) for crystal structures of alkyl isothiocyanates and found 26 hits. The ITC group parameters of these structures were tabulated (Supporting Information Table S8), and basic statistical data obtained for this set of crystal structures are included in the last four rows of Table 3. Extreme γ angles may result because of the formation of antiparallel R−NCS pairs because of the ITC nitrogen's engagement in hydrogen bonding and most frequently because of incipient nucleophilic attack[21−23] of neighboring groups on the ITC carbon. The average of the γ angles is 159.3° with a standard deviation of 10.6°, and these data are fully consistent with the discussion of the potential energy surface of AITC.

2.3. Electronic Structure and N-Hybridization of Organic Isothiocyanates. The N-hybridization of an organic isothiocyanate R−N═C═S is expected to affect the magnetic shieldings of N and C greatly, and Scheme 3 helps to explain. Resonance forms Asp^2 and Bsp^2 describe N-sp^2-hybridized isothiocyanate. Both resonance structures contain one sp^2 lone pair. They differ in that the N-p_π-AO remains a p_π lone pair in the polar resonance form Asp^2, while it engages in π-bond formation in Bsp^2. Their relative contributions determine the polarity of the NC bond and dominate the molecular dipole moment.[24−26] Similarly, resonance forms Asp−Csp describe N-sp-hybridized isothiocyanate, and they reflect whether the *two* N-p_π-AOs remain at N (Asp), whether one engages in π-bond formation (Bsp), or whether both engage in π-bond formation (Csp). Usually, discussions of bent isothiocyanates begin with the consideration of Bsp^2, while discussions of linear structures invoke Csp. Our perspective is preferable because it introduces the unconventional resonance form Bsp to the discussion. In fact, the electronic structure of an isothiocyanate with any angle γ can be described by the interplay between Asp^x and Bsp^x and N-sp^x-hybridization.

DOI: 10.1021/acs.joc.5b00080
J. Org. Chem. 2015, 80, 4360−4369

Scheme 3. Resonance Forms for the Discussion of the Electronic Structure of AITC as a Function of N-Hybridization

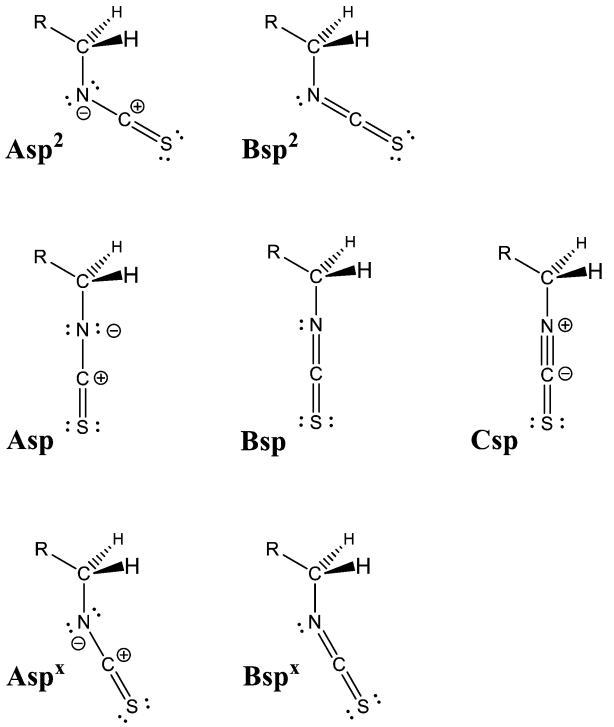

The N-sp-hybridization is advantageous in **A** and **B** as it strengthens the σ-bonds from N to both of the attached C atoms. The N-sp-hybridization may suffer from electron−electron repulsion in the N basin (i.e., the immediate vicinity around N) if the NC(S) bond polarity is high (**A** important). In this case, a high importance of **A** creates a driving force to decrease the γ angle to allow for stabilization of one N lone pair in a σ-orbital.

The structural data for AITC (Table 3) support this interpretation. The minima and the transition state structures show a preference for a γ angle of about 150°. One should *not* be surprised that the γ angles are not ≈120°; the CN(S) bond is polar, and one should expect resonance form **A** to be important. Hence, the only question is whether **A** is important enough to force the γ angle to be less than 180° and by how much. The data in Table 3 allow for a comparison of N-sp-hybridized structures (higher-order saddle points, $\gamma \approx 180°$), N-sp^x-hybridized structures (minima and transition state structures, $\gamma \approx 150°$), and N-sp^2-hybridized structures (with constraint $\gamma = 120°$). The comparison shows significant inverse correlations between the γ angle and the lengths of the C3−N4 and N4−C5 bonds, and that there is hardly any dependence of the C5−S6 bond length on N-hybridization.

2.4. N-sp^x-Hybridization and Chemical Shifts of AITC.

Isotropic NMR chemical shifts were computed with the gauge-independent atomic orbital (GIAO) method for all atoms of minima M1 and M2 for the gas phase and for $CDCl_3$, CD_3OD, and DMSO solutions using the SMD model. Coupling constants also were computed for M1 and M2 in gas phase and in $CDCl_3$ solution. Full results are provided as Supporting Information. The NMR data computed for M1 and M2 align with the measured chemical shift pattern. The C chemical shifts are within 10% of the measured values, and the computations reproduce the solvent shift of δ(C5) relative to δ(C1). The computed NMR data most relevant to the present analysis are collected in Table 5. While the present analysis focuses on ^{13}C

Table 5. Computed NMR Chemical Shifts[a,b]

	M1	M2	CTS	ETS1	ETS2	ICS(sp^x)	SD(sp^x)
C1	119.50	122.76	128.33	119.97	118.56	121.82	3.54
C2	138.16	142.07	139.86	144.65	143.60	141.67	2.38
C3	50.18	51.14	44.66	46.92	47.70	48.12	2.32
C5	144.40	144.36	143.20	142.95	142.01	143.39	0.90
N4	106.29	111.52	113.00	109.22	110.44	110.10	2.27

	SOSP1	SOSP2	TOSP	ICS(sp)	SD(sp)	ΔICS1
C1	119.06	122.54	119.51	120.37	1.55	1.45
C2	138.19	139.99	143.14	140.44	2.04	1.23
C3	46.95	48.71	44.70	46.79	1.64	1.33
C5	132.89	130.23	129.91	131.01	1.33	12.37
N4	96.51	100.04	99.23	98.59	1.51	11.50

	M1$_{120}$	M2$_{120}$	CTS$_{120}$	ETS1$_{120}$	ETS2$_{120}$	ICS(sp^2)	SD(sp^2)	ΔICS2
C1	118.66	122.95	121.48	119.55	117.68	120.06	1.91	1.81
C2	139.20	142.35	142.49	142.33	145.89	142.45	2.12	-0.85
C3	57.98	58.75	59.82	51.10	54.93	56.52	3.16	-8.45
C5	175.47	177.68	177.77	177.42	173.16	176.30	1.78	-32.85
N4	134.87	142.26	141.22	138.83	140.24	139.49	2.57	-29.34

[a]Computed at GIAO(B3LYP/6-311+G(2d,p)//B3LYP/6-311G(d,p)) and given in ppm. [b]C shifts relative to TMS (σ = 182.47 ppm) and N shifts relative to NH_3 (σ = 258.4 ppm).

DOI: 10.1021/acs.joc.5b00080
J. Org. Chem. 2015, 80, 4360−4369

NMR spectra, we are also reporting N chemical shifts and note their good agreement with reported experimental data.[27]

Variations of the γ angle affect the interplay between Asp^x and Bsp^x, and the magnetic shieldings of N4 and C5 reflect these changes. We computed the isotropic chemical shifts (ICS) of C and N atoms in five stationary structures with N-sp^x-hybridization (M1, M2, CTS, ETS1, and ETS2), in three stationary structures with N-sp-hybridization (SOSP1, SOSP2, and TOSP), and in five constrained structures with N-sp^2-hybridization ($M1_{120}$, $M2_{120}$, CTS_{120}, $ETS1_{120}$, and $ETS2_{120}$). The computed isotropic chemical shifts are given in Table 5 together with the average values ICS(sp^x), ICS(sp), and ICS(sp^2) for a given atom in the sets of sp^x-, sp-, and sp^2-hybridized structures, respectively, together with the associated standard deviations SD(sp^x), SD(sp), and SD(sp^2). The values ΔICS1 = ICS(sp^x) − ICS(sp) and ΔICS2 = ICS(sp^x) − ICS(sp^2) inform about the dependency of the NMR chemical shift of a specific atom on the γ angle.

The Larmor frequency ν_L can be measured precisely if a nucleus experiences one magnetic environment for a long time. If a nucleus experiences more than one magnetic environment in a dynamic process,[18c,19c,28] then the uncertainty of its Larmor frequency is related to the lifetime, τ, by $\Delta\nu = h/(2\pi\tau)$. We now need to differentiate between changes of the magnetic environment because of the *exchange dynamics* (i.e., here the isomerization *between* conformations; changes of the dihedral angles α and β) or because of the *molecular dynamics* (i.e., the structural flexibility *within* each isomer; changes of angles γ and ε). The most familiar dynamic exchange scenarios involve the exchange of a given nucleus between magnetic environments due to hindered internal rotation (i.e., amides[29,30]) because of ring inversion (i.e., cyclohexanes,[31] lactones,[32] lactames,[33] azepines[34]) or as the result of tautomerization (i.e., enolization of β-dicarbonyls[35]). These scenarios usually are discussed as a function of the exchange time between the two magnetic environments and with the implicit assumption that the two magnetic environments do not change much: At low temperature, two peaks are observed at ν_A and ν_B, and at high temperatures, one peak is observed at about $(\nu_A + \nu_B)/2$. For AITC, the *conformational dynamics* between M1 and M2 (or M2′) are very fast at every temperature, and the conformer dependence of the chemical shifts is small ($\nu_{M1} - \nu_{M2} < 3$ ppm, vide infra). However, the *molecular dynamics* (i.e., the structural flexibility *within* each conformer) make all the difference for organic isothiocyanates.

Changes in the magnetic environment because of *conformational dynamics* (isomerization *between* conformations) and their magnitudes are described by the values SD(sp^x), SD(sp), and SD(sp^2). For a given N-hybridization, the chemical shift of the C and N nuclei remains within a few ppm (<3 ppm, Table 5).

Changes in the magnetic environment because of *molecular dynamics* (*within* a given conformer) are largely determined by the atom's hybridization, and their magnitudes are described by the values ΔICS1 and ΔICS2. As can be seen, the absolute values of ΔICS1 and ΔICS2 are small for C1 and C2 (<2 ppm) but much larger for N4 and C5 (+10 to −33 ppm).

In the absence of exchange between conformers M1, M2, and M2′, C1 and C2 would give rise to normal peaks because the changes in their magnetic environments are small. In contrast, the nuclei N4 and C5 experience great variability of their magnetic environments in every conformation—ΔICS1 *and* ΔICS2 are large in magnitude—and lifetime broadening will broaden the peaks (or flatten them completely) even in absence of exchange between the minima M1 and M2, and M2′. The ^{13}C NMR spectrum of AITC does show a well-defined peak for C3, and we computed ΔICS1(C3) = 1.3 ppm and ΔICS2(C3) = −8.5 ppm. These data are compatible if deformations from the equilibrium structure into regions with $\gamma > 150°$ are more facile than deformations to structures with $\gamma < 150°$, and this is in line with the relative energies of Table 4.

2.5. Vibrational Dynamics of Allyl Isothiocyanate. There are two kinds of vibrational modes that affect the bond angle at N, and these are the γ and ε bending modes (Scheme 4). The γ bending modes move the NCS group as a whole relative to the R group. The potential energy surface is rather flat with regard to changes of the N-hybridization by γ bending: $\nu_2(\gamma)$ = 60 cm^{-1} and $\nu_4(\gamma)$ = 246 cm^{-1} in M1 and $\nu_2(\gamma)$ = 69 cm^{-1} and $\nu_4(\gamma)$ = 340 cm^{-1} in M2. The periods of these γ bending vibrations are between 560 and 95 fs. The ε bending modes move the ITC carbon out of the near-linear NCS group and thereby change the γ angle. In M1, C5 moves out of the (C3,N4,S6) plane with $\nu_5(\varepsilon)$ = 450 cm^{-1} and C5 moves in that plane with $\nu_6(\varepsilon)$ = 478 cm^{-1}. In M2, C5 moves out of the (C3,N4,S6) plane with $\nu_6(\varepsilon)$ = 449 cm^{-1} and in that plane with $\nu_7(\varepsilon)$ = 498 cm^{-1}. The periods of these out-of-plane or in-plane vibrations are about 70 or 66.7 fs, respectively. The limits for the accessible range of the γ angle are determined by the positive reinforcement of the γ and ε bending modes. To estimate this range, one needs to follow the trajectories at least long enough for $\nu_2(\gamma)$ to go through a full cycle.

Scheme 4. Schematic Drawings of the γ and ε Bending Modes of Conformation M1

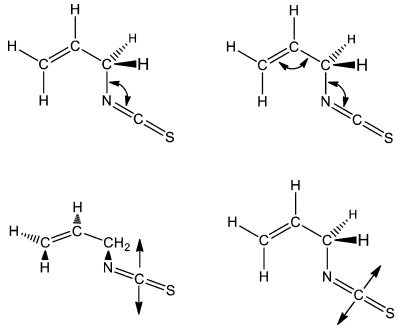

The molecular dynamics of the minima M1 and M2 of AITC were studied with the atom-centered density matrix propagation (ADMP) molecular dynamics method at the B3LYP/6-31G(d,p) level. The structures of the minima are very similar at the levels B3LYP/6-31G(d,p) and B3LYP/6-311G(d,p). The trajectory was started either at M1 (γ = 149.6°, ε = 175.7°, δ = 180°) or M2 (γ = 149.7°, ε = 175.4°, δ = 179.1°) and followed for 1 ps with a step size of 0.2 fs. Figure 4 shows the variations of the bond angle $\varepsilon = \angle$(N4−C5−S6), and Figure 5 shows the variations of the angle $\gamma = \angle$(C3−N4−C5) along the same trajectories.

The periodicities of the ε-ITC bending modes of about 70 fs are clearly reflected in Figures 4 and 5. The trajectories shown in Figure 4 show a modest variability of the ε angle in the range of 155° < ε < 180°. The γ bending modes may place the ITC moiety anywhere inside a circular sector around the (N···S) axis of the ITC group of M1 (or M2), a sector which originates at N and has its chord length determined by the amplitude of the $\nu_2(\gamma)$ mode. While γ bending modes move the ITC group (as a

DOI: 10.1021/acs.joc.5b00080
J. Org. Chem. 2015, 80, 4360−4369

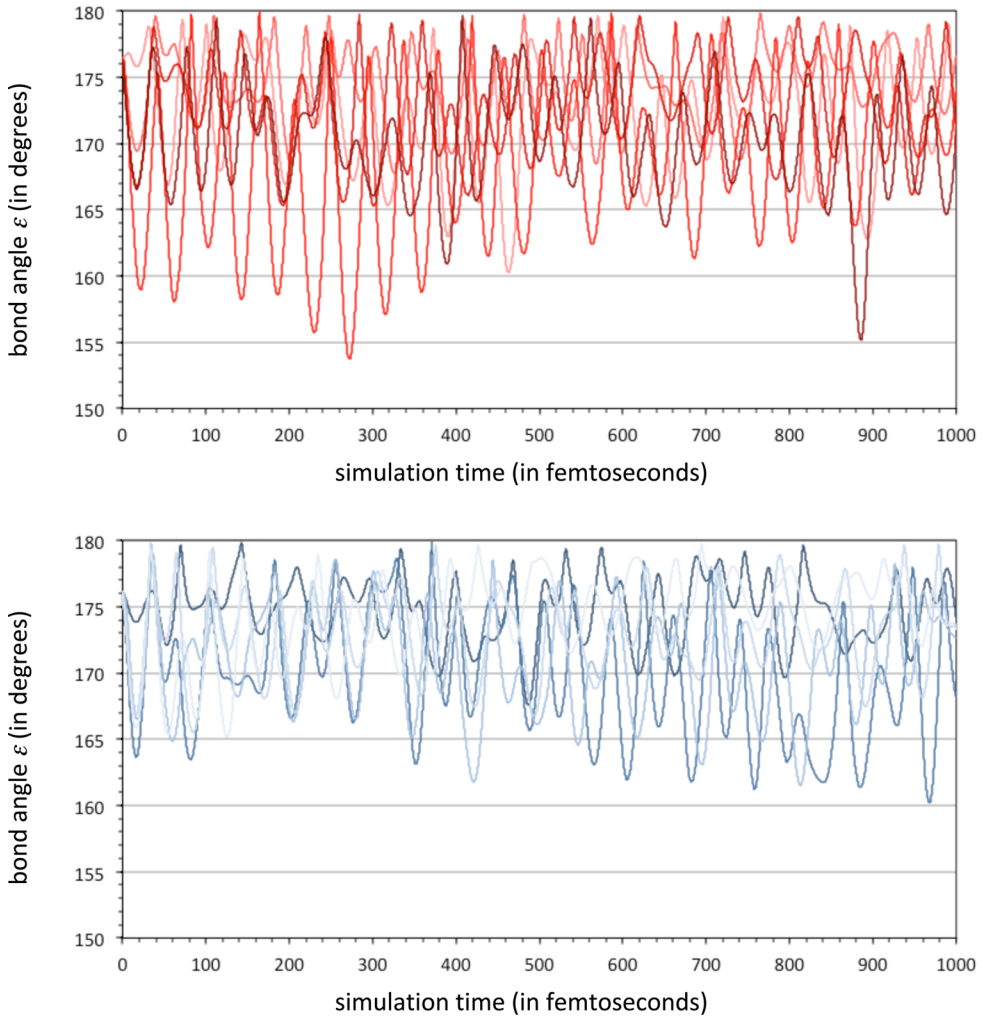

Figure 4. Variations of the bond angle $\varepsilon = \angle(\text{N4}-\text{C5}-\text{S6})$ of AITC along trajectories computed with the ADMP method at the B3LYP/6-31G(d,p) level. Trajectories starting at M1 ($\varepsilon = 175.7°$) are shown on top (red), and those starting at M2 ($\varepsilon = 175.4°$) are shown on the bottom (blue).

whole) inside this sector, the ε bending modes move C5 out of the (N···S) axis. For the M1 conformation, the ε bending modes may place C5 anywhere inside an ellipsoid around the ITC group, which is approximately centered at C5(M1), squashed along the (N···S) axis, and whose other two axes are determined by the amplitudes of the $\nu_5(\varepsilon)$ and $\nu_6(\varepsilon)$ modes, respectively. It is this combination of the γ and ε bending modes which results in the rather high variability of the γ angles: Figure 5 shows that the γ angles vary in the wide range of $120° < \gamma < 180°$ and that every path traced out on the potential energy surface depends greatly on the phase of the vibrations.

We explored the potential energy surface of AITC in the vicinities of M1 and M2 and determined isotropic chemical shifts ICS(γ) as a function of the γ angle (in three discrete regions). The next level of sophistication would involve the mapping of the potential energy surface as a function of the bond angles γ and ε and the determination of isotropic chemical shifts ICS(γ,ε) for a matrix of structures AITC(γ,ε). Further refinements would include more and more internal coordinates that affect the shielding of C5, and all this could be done. However, the large magnitude of the computed ΔICS(γ) values and the realization that the trajectories can follow a great many paths on the potential energy surface PES(γ,ε,...) suffice to explain the very broad distribution of the Larmor frequencies of individual nuclei in the magnetic environments around every conformer structure.

3. CONCLUSION

The ^{1}H and ^{13}C NMR spectra of allyl isothiocyanate were measured in several solvents. Interestingly, the isothiocyanate carbon (C5) is nearly silent in the ^{13}C NMR spectrum of AITC, and a brief review of the literature showed this phenomenon to be common for organic isothiocyanates R–N=C=S. Dynamic effects on the ^{13}C NMR spectrum of AITC were studied with potential energy surface analyses, magnetic shielding computations, and molecular dynamics methods. Specifically, the structural, energetic, and electronic effects of variations of the N-hybridization have been explored, and the changes of the magnetic environment have been described, which occur because of the *exchange dynamics* (i.e., exchange between conformations; changes of the dihedral angles α and β) or because of the *molecular dynamics* (i.e., structural flexibility within each isomer; changes of bond angles γ and ε).

The conformational space of AITC contains two types of minima: C_s-symmetric M1 and a pair of enantiomers M2 and M2′. Exchange between conformations M1 and M2 or M2′ via transition state structures CTS and CTS′ and enantiomerization M2 ⇄ M2′ via transition state structures ETS1 or ETS2

DOI: 10.1021/acs.joc.5b00080
J. Org. Chem. 2015, 80, 4360–4369

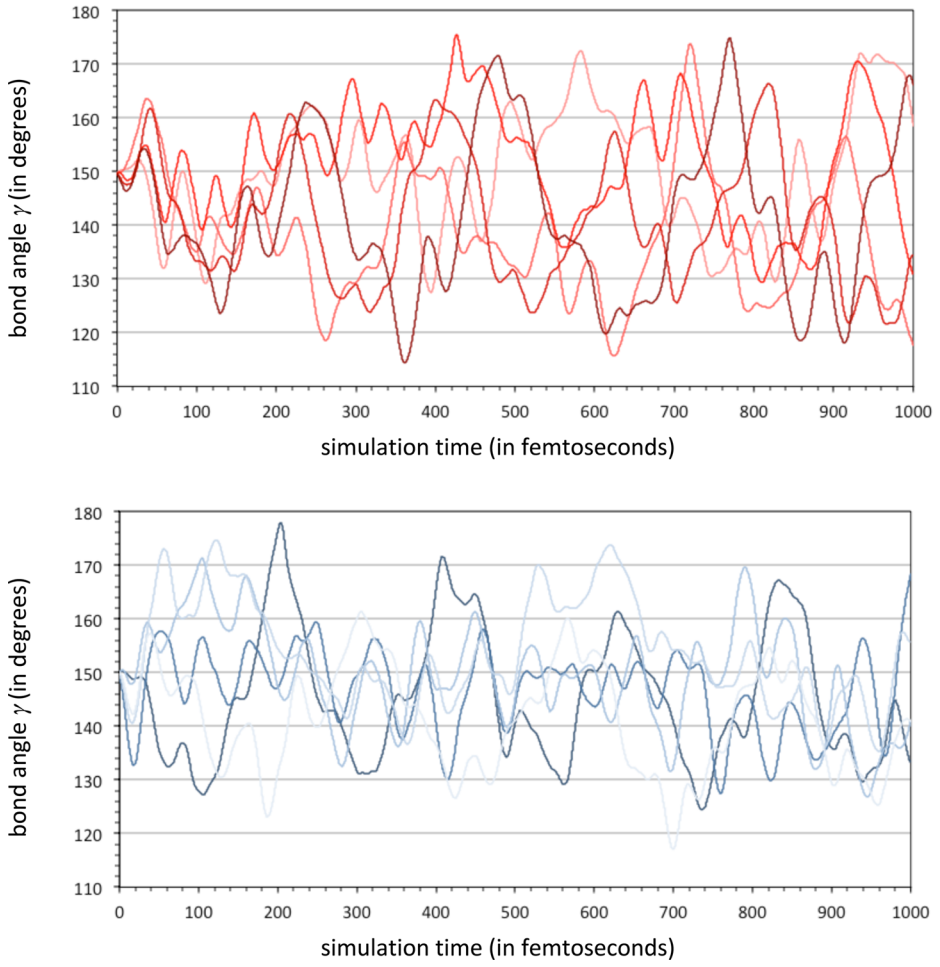

Figure 5. Variations of the angle $\gamma = \angle$(C3−N4−C5) of AITC along trajectories computed with the ADMP method at the B3LYP/6-31G(d,p) level. Trajectories starting at M1 (γ = 149.6°) are shown on top (red), and those starting at M2 (γ = 149.7°) are shown on the bottom (blue).

involve simultaneous rotations about the C2−C3 bond (dihedral angle α) and the C3−N4 bond (dihedral angle β). The minima and all structures along the intrinsic reaction paths connecting minima and transition states feature angles at N ($\gamma \approx 150°$) that are indicative of sp^x-hybridization with $1 < x < 2$. However, studies of stationary structures with N-sp-hybridization ($\gamma \approx 180°$) and of model structures with N-sp^2-hybridization ($\gamma = 120°$) show that AITC can access a much larger region of the potential energy surface.

The exchange dynamics between conformers are fast even at very low temperature, and conformational effects on ^{13}C chemical shifts are rather small ($\nu_{M1} - \nu_{M2} < 3$ ppm). This is true for structures with the preferred N-sp^x-hybridization ($1 < x < 2$, $\gamma \approx 150°$), and it is also true for structures with N-sp- ($\gamma \approx 180°$) or N-sp^2- ($\gamma \approx 120°$) hybridization.

The dynamic effects observed by ^{13}C NMR spectroscopy reflect the facile changes of the bond angles at N4 (γ) and C5 (ε) in every conformer. We determined isotropic chemical shifts ICS(γ) as a function of the γ angle for sp, sp^x, and sp^2 N-hybridization. The parameters ΔICS1 = ICS(sp^x) − ICS(sp) and ΔICS2 = ICS(sp^x) − ICS(sp^2) quantify the γ angle dependency of the NMR chemical shift of a specific nucleus, and their values show especially large effects for the N and C atoms of the ITC functional group (10−33 ppm). The accessible range of the bond angle γ is largely determined by the superposition of the γ and ε bending modes, and the computed molecular dynamics trajectories show that every conformation of AITC can access a large region of the potential energy surface AITC(γ,ε,...) with γ angles in the wide range of $120° < \gamma < 180°$ and ε angles in the more modest range of $155° < \varepsilon < 180°$.

The large magnitude of the computed ΔICS(γ) values explains the very broad distribution of the Larmor frequencies of individual ITC carbon nuclei in the vicinity of every conformer. Because the extreme broadening of the ^{13}C NMR signal of the ITC carbon is caused by the structural flexibility of every conformer, the analysis of AITC provides a general explanation for the near-silence of the ITC carbon in ^{13}C NMR spectra of unaggregated and sterically unencumbered organic isothiocyanates.

4. EXPERIMENTAL AND COMPUTATIONAL DETAILS

4.1. NMR Spectroscopy. Allyl isothiocyanate was obtained from Sigma-Aldrich (95%). The spectra were measured in Cambridge isotope solvents at 0.3 M concentrations with a 500 MHz spectrometer operating with a cryogenically chilled HCN probe. Chemical shifts are given relative to tetramethylsilane (TMS).

4.2. Computational Details. The potential energy surface of AITC was explored with the hybrid density functional method B3LYP[36,37] with the 6-311G(d,p) basis set.[38−40] Stationary structures were completely optimized,[41] and some structures were optimized with constraints imposed (vide supra). Analytical frequencies were computed to characterize the nature of the stationary structure and to determine the thermochemistry. Isotropic NMR chemical shifts were computed with the GIAO method[42,43] using the 6-311+G(2d,p) basis

DOI: 10.1021/acs.joc.5b00080
J. Org. Chem. 2015, 80, 4360−4369

set[39,40] and the B3LYP/6-311G(d,p) structures, that is, the B3LYP/6-311+G(2d,p)//B3LYP/6-311G(d,p) level. Chemical shifts are reported with reference to TMS (H and C NMR) or ammonia (N NMR). Solvent effects on isotropic NMR chemical shifts were explored for the minima using the SMD model:[44] GIAO(SMD(B3LYP/6-311+G(2d,p))//B3LYP/6-311G(d,p)). Coupling constants were determined for the gas phase and for $CDCl_3$ solution with the SMD method.[45] Trajectories were computed using the ADMP molecular dynamics model[46] at the B3LYP/6-31G(d,p) level.

■ ASSOCIATED CONTENT

Supporting Information

^1H and ^{13}C NMR spectra of AITC in $CDCl_3$, CD_3OD, and DMSO-d_6 including DEPT135, HMBC, and HSQC spectra. Cartesian coordinates of optimized structures. Computed NMR shielding values of M1 and M2 (Tables S6 and S7). Matrices of computed spin−spin coupling constants J (Hz) for M1 and M2. Summary of structural parameters of ITC groups in crystal structures of alkyl isothiocyanates (Table S8). Figure S4b shows the variations of the dihedral angle $\delta = \angle$(C3−N4−C5−S6) of AITC along the trajectories of Figure 4. This material is available free of charge via the Internet at http://pubs.acs.org.

■ AUTHOR INFORMATION

Corresponding Author

*E-mail: glaserr@missouri.edu.

Notes

The authors declare no competing financial interest.

■ ACKNOWLEDGMENTS

Acknowledgment is made to the donors of the American Chemical Society Petroleum Research Fund for partial support of this research. The 600 MHz spectrometer was purchased with support by the National Science Foundation (NSF DBI-0070359).

■ REFERENCES

(1) Ullah, M. F.; Bhat, S. H.; Husain, E.; Abu-Duhier, F.; Hadi, S. M.; Sarkar, F. H.; Ahmad, A. *Phytochem. Rev.* **2014**, *13*, 811−833.

(2) Citi, V.; Martelli, A.; Testai, L.; Marino, A.; Breschi, M. C.; Calderone, V. *Planta Med.* **2014**, *80*, 610−613.

(3) Montaut, S.; Bleeker, R. S. *J. Ethnopharmacol.* **2013**, *149*, 401−408.

(4) Ioannides, C.; Hanlon, N.; Konsue, N. *Open Nutraceuticals J.* **2010**, *3*, 55−62.

(5) Leoncini, E.; Malaguti, M.; Angeloni, C.; Motori, E.; Fabbri, D.; Hrelia, S. *J. Food Sci.* **2011**, *76*, H175-81.

(6) Kelsey, N. A.; Wilkins, H. M.; Linseman, D. A. *Molecules* **2010**, *15*, 7792−7814.

(7) Mori, N.; Kurate, M.; Yamazaki, K.; Hosokawa, H.; Nadamoto, T.; Inoue, K.; Fushiki, T. *J. Nutr. Sci. Vitaminol.* **2013**, *59*, 56−63.

(8) Abbaoui, B.; Riedl, K. M.; Ralston, R. A.; Thomas-Ahner, J. M.; Schwartz, S. J.; Clinton, S. K.; Mortazavi, A. *Mol. Nutr. Food Res.* **2012**, *56*, 1675−1687.

(9) Hong, F.; Freeman, M. L.; Liebler, D. C. *Chem. Res. Toxicol.* **2005**, *18*, 1917−1926.

(10) Sigma-Aldrich Product Catalog. Spectra are accessible by adding the product number at the end of the URL http://www.sigmaaldrich.com/catalog/product/aldrich/. For example, to access information about butyl isothiocyanate (product number 253790), enter http://www.sigmaaldrich.com/catalog/product/aldrich/253790 in the URL field of your browser. All of the cited compounds were accessed 10/11/2014.

(11) SDBSWeb, National Institute of Advanced Industrial Science and Technology (AIST), http://sdbs.db.aist.go.jp. All of the cited compounds were accessed 11/11/2014.

(12) (a) Phenyl isothiocyanate: 139742 in ref 10. (b) *m*-Tolyl isothiocyanate: 19528 in ref 10. (c) *p*-Tolyl isothiocyanate: 23399 in ref 10. (d) *o*-Tolyl isothiocyanate: 25187 in ref 10.

(13) Benzyl isothiocyanate: 252492 in ref 10.

(14) Butyl isothiocyanate: 253790 in ref 10; 10207 in ref 11.

(15) Propyl isothiocyanate: 253944 in ref 10; 21756 in ref 11.

(16) Jones, R. G.; Allen, G. *Org. Magn. Reson.* **1982**, *19*, 196−203.

(17) Giffard, M.; Cousseau, J.; Martin, G. J. *J. Chem. Soc., Perkin Trans. 2* **1985**, 157−160.

(18) (a) Günther, H. *NMR Spectroscopy: Basic Principles, Concepts and Applications in Chemistry*, 3rd ed.; Wiley-VCH: Weinheim, Germany, 2013. (b) Chapter 11 in ref 18a, Carbon-13 Nuclear Magnetic Resonance Spectroscopy. (c) Chapter 13 in ref 18a, Influence of Dynamic Effects on Nuclear Magnetic Resonance Spectra.

(19) (a) Friebolin, H. *Basic One- and Two-Dimensional NMR Spectroscopy*, 1st ed.; Wiley-VCH: Weinheim, Germany, 2010. (b) Chapter 9 in ref 19a, Two-Dimensional NMR Spectroscopy. (c) Chapter 11 in ref 19a, Dynamic NMR Spectroscopy (DNMR).

(20) Allen, F. H. *Acta Crystallogr.* **2002**, *B58*, 380−388.

(21) Brennan, R. G.; Prive, G. G.; Blonski, W. J. P.; Hruska, F. E.; Sundaralingam, M. *J. Am. Chem. Soc.* **1983**, *105*, 7737−7742.

(22) Wallis, J. D.; Dunitz, J. D. *Chem. Commun.* **1984**, 671−672.

(23) Glaser, R.; Horan, C. J.; Nelson, E. D.; Hall, M. K. *J. Org. Chem.* **1992**, *57*, 215−228.

(24) Koput, J. *J. Mol. Spectrosc.* **1988**, *127*, 51−60.

(25) Zheng, C.; Guirgis, G. A.; Deeb, H.; Durig, J. R. *J. Mol. Struct.* **2007**, *829*, 88−110.

(26) Durig, J. A.; Zhou, X.; Defrawy, A. M. E.; Guirgis, G. A.; Gounev, T. K.; Zheng, C. *J. Mol. Struct.* **2007**, *839*, 107−124.

(27) Compare Table 1 in ref 17. The nitrogen chemical shifts in R−NCS (R = Me, Bu, Ph, vinyl) are −260 to −290 ppm relative to external nitromethane, and H_3C-NO_2 appears at 380.2 ppm relative to NH_3.

(28) Levitt, M. H. Motion and Relaxation. Part 7 in *Spin Dynamics: Basics of Nuclear Magnetic Resonance*, 2nd ed.; Wiley-VCH: Weinheim, Germany, 2008.

(29) Gutowsky, H. S.; Holm, C. H. *J. Chem. Phys.* **1956**, *25*, 1228−1234.

(30) Wiberg, K. B.; Rablen, P. R.; Rush, D. J.; Keith, T. A. *J. Am. Chem. Soc.* **1995**, *117*, 4261−4270.

(31) Anet, F. A. L.; Bourn, A. J. R. *J. Am. Chem. Soc.* **1967**, *89*, 760−768.

(32) Marell, D. J.; Emond, S. J.; Kulshrestha, A.; Hoye, T. R. *J. Org. Chem.* **2014**, *79*, 752−758.

(33) Witosinska, A.; Musielak, B.; Serda, P.; Owinska, M.; Rys, B. *J. Org. Chem.* **2012**, *77*, 9784−9794.

(34) Ramig, K.; Greer, E. M.; Szalda, D. J.; Karimi, S.; Ko, A.; Boulos, L.; Gu, J.; Dvorkin, N.; Bhramdat, H.; Subramaniam, G. *J. Org. Chem.* **2013**, *78*, 8028−8036.

(35) Lacerda, V.; Constantino, M. G.; da Silva, G. V. J.; Neto, Á. C.; Tormena, C. F. *J. Mol. Struct.* **2007**, *828*, 54−58.

(36) Sholl, D. S.; Steckel, J. A. *Density Functional Theory: A Practical Introduction*, 1st ed.; Wiley: New York, 2009.

(37) Engel, E.; Dreizler, R. M. *Density Functional Theory: An Advanced Course*; Springer: Berlin, 2011.

(38) Frisch, M. J.; Trucks, G. W.; Schlegel, H. B.; Scuseria, G. E.; Robb, M. A.; Cheeseman, J. R.; Scalmani, G.; Barone, V.; Mennucci, B.; Petersson, G. A.; Nakatsuji, H.; Caricato, M.; Li, X.; Hratchian, H. P.; Izmaylov, A. F.; Bloino, J.; Zheng, G.; Sonnenberg, J. L.; Hada, M.; Ehara, M.; Toyota, K.; Fukuda, R.; Hasegawa, J.; Ishida, M.; Nakajima, T.; Honda, Y.; Kitao, O.; Nakai, H.; Vreven, T.; Montgomery, J. A. Jr.; Peralta, J. E.; Ogliaro, F.; Bearpark, M.; Heyd, J. J.; Brothers, E.; Kudin, K. N.; Staroverov, V. N.; Keith, T.; Kobayashi, R.; Normand, J.; Raghavachari, K.; Rendell, A.; Burant, J. C.; Iyengar, S. S.; Tomasi, J.; Cossi, M.; Rega, N.; Millam, J. M.; Klene, M.; Knox, J. E.; Cross, J. B.; Bakken, V.; Adamo, C.; Jaramillo, J.; Gomperts, R.; Stratmann, R. E.; Yazyev, O.; Austin, A. J.; Cammi, R.; Pomelli, C.; Ochterski, J. W.; Martin, R. L.; Morokuma, K.; Zakrzewski, V. G.; Voth, G. A.; Salvador, P.; Dannenberg, J. J.; Dapprich, S.; Daniels, A. D.; Farkas, O.;

DOI: 10.1021/acs.joc.5b00080
J. Org. Chem. 2015, 80, 4360−4369

Foresman, J. B.; Ortiz, J. V.; Cioslowski, J.; Fox, D. J. *Gaussian 09*, revision D.01; Gaussian, Inc.: Wallingford, CT, 2013.
(39) Schuchardt, K. L.; Didier, B. T.; Elsethagen, T.; Sun, L.; Gurumoorthi, V.; Chase, J.; Li, J.; Windus, T. L. *J. Chem. Inf. Model.* **2007**, *47*, 1045−1052 https://bse.pnl.gov/bse/portal (accessed 11/15/14).
(40) *Gaussian 09 Users' Reference*; http://www.gaussian.com/g_tech/g_ur/m_basis_sets.htm (accessed 11/15/14).
(41) Peng, C.; Ayala, P. Y.; Schlegel, H. B.; Frisch, M. J. *J. Comput. Chem.* **1996**, *17*, 49−56.
(42) Cheeseman, J. R.; Trucks, G. W.; Keith, T. A.; Frisch, M. A. *J. Chem. Phys.* **1996**, *104*, 5497−5509.
(43) Wiitala, K. W.; Hoye, T. R.; Cramer, C. J. *J. Chem. Theory Comput.* **2006**, *2*, 1085−1092.
(44) Marenich, A. V.; Cramer, C. J.; Truhlar, D. G. *J. Phys. Chem. B* **2009**, *113*, 6378−6396.
(45) Deng, W.; Cheeseman, J. R.; Frisch, M. J. *J. Chem. Theory Comput.* **2006**, *2*, 1028−1037.
(46) Schlegel, H. B.; Iyengar, S. S.; Li, X.; Millam, J. M.; Voth, G. A.; Scuseria, G. E.; Frisch, M. J. *J. Chem. Phys.* **2002**, *117*, 8694−8704.

DOI: 10.1021/acs.joc.5b00080
J. Org. Chem. 2015, 80, 4360−4369